RSC Sustainability

ROYAL SOCIETY OF CHEMISTRY

PAPER

View Article Online
View Journal

Cite this: DOI: 10.1039/d5su00850f

Nickel extraction from olivine using waste acid from an electrochemical marine CO_2 removal process

Alexander J. Robinson, [a] Dan Thien Nguyen,[b] Brady Anderson,[c] Jian Liu, [c] Pravalika Butreddy, [b] Elias Nakouzi, [bd] Qingpu Wang, [b] Paul Marsh[c] and Chinmayee V. Subban *[ac]

Global production of nickel (Ni) and ferronickel (FeNi) alloys, critical to battery materials and stainless steel alloys, is limited to a few countries due to the distribution of laterite ores. To meet the growing demand, an alternative supply of Ni and FeNi alloys needs to be established. Laterite ores result from olivine ($Mg_xFe_{2-x}SiO_4$) weathering under tropical conditions, making olivine a promising alternative source to consider; however, the lower Ni concentration of olivine makes it less economical. One approach to lowering the process costs is using waste chemical inputs in place of expensive commodity chemicals. In this study we evaluate the feasibility of using such waste byproducts generated by a demonstration-scale electrochemical marine carbon dioxide removal system to extract Ni from olivine (0.27 wt% Ni) as FeNi alloy. Bipolar membrane electrodialysis (BPMED) technology used for ocean alkalinity enhancement generates acidic, desalinated, and basic streams using seawater and electricity. The acid stream is a waste product, and we show that it is 37% better than equal-strength commercial HCl for leaching of Ni from olivine at room temperature. A small volume of the alkaline product from BPMED is used to increase the pH of the olivine leachate to remove all dissolved silicon and the majority of the dissolved iron, while retaining most of the dissolved Ni (65%) and Mg (84%). This enriched solution is used for Ni recovery *via* electroplating while the spent electrolyte, rich in Mg, is suitable as an additional source of alkalinity for marine CO_2 removal. We demonstrate the recovery of Ni as a FeNi alloy with an Fe to Ni molar ratio of 1.37 : 1 and evaluate the cost-benefit of the process for various possible scenarios. Preliminary assessment indicates an overall net economic benefit from recovering Ni from olivine using the proposed method and the net benefit is expected to further increase if the overall recovery rate of Ni is improved, the price of the Ni product is increased, and the value of CO_2 credit is included.

Received 7th November 2025
Accepted 24th November 2025

DOI: 10.1039/d5su00850f

rsc.li/rscsus

Sustainability spotlight

Global production of nickel, critical to battery materials and stainless-steel alloys, is limited to a few countries. To meet the growing demand, an alternative supply of nickel is needed. Olivine is a widely available mineral, but its low nickel concentration makes it less economical to process. We demonstrate the feasibility of using waste acid from an electrochemical marine carbon dioxide removal system to extract nickel as Fe–Ni alloy *via* electroplating. The only waste stream from the process is Mg-rich and can be utilized to achieve additional marine CO_2 removal. Preliminary assessment indicates an overall net economic benefit from recovering nickel from olivine using the proposed method, highlighting the feasibility of integrating emerging technologies for sustainable development.

1. Introduction

An increase in electrification across sectors, especially transportation, has significantly increased the demand for batteries. Growing demand for batteries translates to an increase in demand for battery materials such as nickel (Ni).[1] The combination of anticipated growth in demand and the current limited global supply chain has placed Ni in the United States Department of Energy's (DOE) highest priority critical mineral category.[2] Similarly, the European Union has prioritized Ni under its Critical Raw Materials Act (CRMA).[3] Current global Ni production through laterite and sulfide ores is largely limited to a few countries,[4] and such dependence risks major economic repercussions if the supply from any of them is disrupted by global

[a]Department of Materials Science and Engineering, University of Washington, WA, USA
[b]Physical and Computational Sciences Directorate, Pacific Northwest National Laboratory, WA, USA
[c]Energy and Environment Directorate, Pacific Northwest National Laboratory, WA, USA. E-mail: chinmayee.subban@pnnl.gov
[d]Department of Chemical Engineering, University of Washington, Seattle, WA, USA

events or national policy.[4,5] The primary demand drivers for Ni are rechargeable batteries that use Ni-based-electrodes and stainless steel production that uses FeNi alloys.[6] There is hence a need for developing alternative Ni sources, both from mineral ores and recycling streams.

One potential untapped mineral resource for Ni is olivine. The weathering of ultramafic rocks such as olivine and serpentines in tropical locations is known to form enriched Ni laterite ores.[7–9] The weathering process in these tropical regions allows for the up-concentration of Ni in these deposits from the original olivine rocks. In non-tropical locations, lower Ni concentration olivine presents itself as the best available primary source. Ni in olivine rocks is known to typically vary between 0.05 and 0.5 wt% which falls short of mined Ni laterites that typically consist of deposits between 1 and 2 wt% Ni.[10,11] This disparity in Ni concentrations makes olivine not cost-competitive as a primary source with current production methods and would require pairing with other technologies to make it a viable Ni source.

Past literature dedicated to extracting Ni from olivine has primarily focused on greener extraction pathways or adding an additional co-benefit to reduce cost.[12–18] Early attempts at Ni extraction sought to boost the leaching efficiency of olivine to provide solutions with higher Ni content.[12,13] One study reported a bioleaching route which preferentially leached Ni, unlike the leaching behavior observed with mineral acids.[12,13,18] This preferential leaching could provide an avenue for reduced processing cost but the overall slow rate of the bioleaching makes it difficult to deploy at large scales. Another method to increase the leaching efficiency of olivine is to chemically convert the silicate rock into a carbonate.[13] By performing a carbonation pretreatment, the leaching efficiency is enhanced over that of fresh olivine rock. Prior studies have demonstrated simultaneous CO_2 mineralization and Ni recovery as NiS.[14–17] While this process has shown promise, preliminary cost–benefit analysis suggests that it is uneconomical compared to conventional mining of laterite ores.[16] More recently, a solvent extraction method for Ni recovery from olivine has been reported that generates additional value streams of silica and iron.[18] In general, due to the relatively low amount of Ni in olivine, the feasibility of Ni extraction from olivine requires integrating it with processes generating additional revenue streams such as co-production of other minerals, generation of chemical co-products, or CO_2 sequestration.

Commercial Ni-recovery from olivine would require accelerated mineral dissolution to meet the minimum process scale needed for economic viability. A common practice is acid digestion and leaching to accelerate the release of critical elements from natural minerals.[19] However, acid use and the neutralization and disposal of the resulting waste streams can add significantly to process costs. In this context, utilization of waste acid streams and steps to minimize waste processing are desirable.

In this study, we evaluate integrating Ni recovery from olivine by utilizing one such waste acid stream. We use acid generated by a demonstration-scale bipolar membrane electrodialysis (BPMED) system deployed for ocean alkalinity enhancement (OAE) in Sequim, WA.[20] The BPMED system consists of alternating bipolar, anion-exchange, and cation-exchange membranes and uses electricity to convert seawater into acidic, alkaline, and desalinated product streams.[21] The alkaline and desalinated streams are used for OAE while the acidic stream is a waste byproduct that requires disposal or alternative use.[20,22–25] To accelerate the dissolution of olivine, we used the waste acid, and subsequently used a fraction of the alkaline product from the BPMED to selectively recover a Ni-rich stream from which we electroplate the Ni (Fig. 1). While the use of olivine to neutralize acidic waste streams from electrochemical processes such as BPMED has previously been reported in the literature,[23,26] mineral extraction from the process has not been widely investigated. Furthermore, olivine has been successfully used for OAE,[27–30] but concerns around bioconcentration of trace elements such as Ni and Cr remain.[31] Extracting Ni prior to OAE addresses a key barrier to safe and sustainable use of olivine, while also generating a value stream.

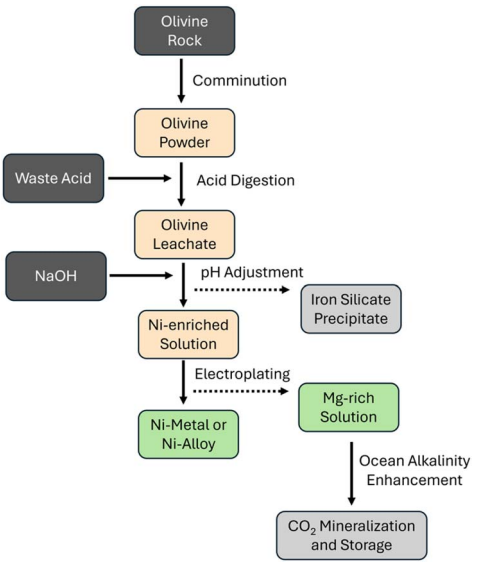

Fig. 1 Process flow diagram showing the production of Ni-metal or Ni-alloy from olivine rock utilizing acid generated from a bipolar membrane electrodialysis system. A beneficial co-product of Mg-rich solution is generated with potential for ocean alkalinity enhancement.

In this study, olivine is first digested with BPMED acid to produce a leachate. The pH of the leachate is then adjusted using NaOH base to precipitate Fe and Si, leaving behind a Mg- and Ni-enriched solution. The Ni is electroplated from this solution and the remaining solution rich in Mg is retained and is suitable for OAE. Given that Mg-based OAE has been widely researched and demonstrated at scale,[32–34] here we focus our efforts primarily on the Ni recovery from olivine and not on OAE.

2. Experimental

2.1 Materials characterization and feedstock preparation

Olivine rock dust was acquired from a commercial vendor (CGG Distributing, Utah USA) and its composition was characterized by inductively coupled plasma-mass spectrometry (ICP-MS)

after digesting in concentrated HNO_3 acid at 70 °C. The samples were characterized for crystallinity using powder X-ray diffraction (XRD) with a Bruker D8 Discover Microfocus system, with a Cu Kα X-ray source. Pattern matching and identification were performed using commercial JADE software. The samples were characterized using a ThermoFisher Scientific Apreo 2 scanning electron microscope (SEM) for morphology and an Oxford Instruments energy dispersive spectroscopy (EDS) system for average elemental distribution. The average particle size of the olivine was determined using a laser-diffraction particle size analyzer (Bettersizer 2600). The BPMED acid and base were collected from Ebb Carbon's demonstration system at PNNL-Sequim,[35,36] and characterized for pH (Mettler Toledo SevenCompact) and composition (ICP-OES; PerkinElmer Optima 7300 DV). The olivine feedstock composition and percent olivine dissolution were determined by ICP-MS (Thermo Scientific iCAP Q). The olivine leachate was prepared by dissolving 15 g L^{-1} olivine in BPMED generated acid over a period of 2 weeks. Residual solid was removed by centrifugation.

2.2. Olivine leaching experiments

The effectiveness of BPMED generated acid to digest olivine was compared with that of commercial acid by digesting olivine in an equivalent pH solution of commercial HCl (prepared from concentrated HCl, Millipore). Olivine was loaded at 2 g L^{-1} in 50 mL solutions with 0.1 mL aliquots taken from the solution at the time intervals of 1 hour, 3 hours, 7 hours, and 24 hours to track the progress of the dissolution. These aliquots were diluted with HNO_3 (nitric acid 70%, Optima™, for Ultra Trace Elemental Analysis, Fisher Chemical) and ultrapure water (18.2 MΩ cm) to create 1% HNO_3 acid solutions within the calibrated concentration range of the ICP-MS instrument. A calibration curve was generated by creating standard solutions of 0.1, 1, 10, 100, and 1000 ppb from a custom Inorganic Standard (HPS-275-019-250) from High Purity Standards and a Si standard (CGSI10) obtained from Inorganic Ventures. The Qtegra software used this calibration curve to report concentration values for the measured analytes. The measured concentration values from the instrument were then adjusted by subtracting the blank and then multiplying by the dilution factor for each sample to get the analyte concentration within each sample. Percent dissolution was determined for each cation by dividing the observed concentration by the theoretical maximum concentration determined from 100% dissolution of olivine. To ensure consistency of ICP-MS measurements, an internal standard of 100 ppb indium was added to each solution to monitor instrument drift over the course of the measurement. Further details of ICP-MS sample preparation and analysis methods are provided in the SI.

2.3 Generation of Ni- and Mg-rich leachate

Olivine leachate exposure to base was initially monitored by generating a titration curve up to a pH of ~6. Titration was conducted by adding 20 μL of 4 M NaOH (prepared from ≥98% reagent grade pellets, Sigma-Aldrich) solution at a time and allowing the pH to equilibrate between additions. Using this data, feedstock solutions at pH 2, 3, 4, 5, and 6 were generated for analysis by ICP-MS while the precipitated solid was analyzed by powder XRD, SEM, and EDS. Based on the ICP-MS results, the pH adjustment methods were insufficient to fully remove Fe without impacting Ni concentration. Further treatment by heating solution at 80 °C for 6 hours precipitated more Fe, thereby leaving a solution concentrated in Ni and Mg which was used for Ni recovery *via* electrodeposition.

2.4 Electrodeposition of Ni

The pH adjusted solution concentrated in Ni and Mg was used as electrolyte for Ni recovery. Ni electroplating is a well-established process used at an industrial scale.[37] In this study we use the approach to show the feasibility of going from mineral to metal. Electroplating experiments used a 3-electorde cell with a platinum (Pt) strip cathode on which the Ni was plated, a Pt wire as the counter electrode, and a Ag/AgCl reference electrode. The voltage was swept between −0.8 V and 0.3 V *vs.* Ag/AgCl at a scan rate of 10 mV s^{-1}. The cathode surface was characterized by X-ray photoelectron spectroscopy (XPS; Kratos Axis Ultra DLD spectrometer equipped with an Al Kα monochromatic X-ray source (1486.6 eV)) and optical microscopy (Keyence Digital Microscope VHX-X1).

2.5 Cost-benefit analysis

This process utilizes the waste acid stream from the BPMED process to extract Ni from olivine contained in ultramafic ore. A net benefit was calculated based on the total benefits from the Ni product and the total costs of energy, materials, and equipment. The potential for CO_2 emission reduction was estimated, but the benefits of carbon credit are not included for the base case. Note that while there is extensive on-going work on BPMED-based OAE,[38] the technology is still in an early demonstration phase. The first-of-a-kind BPMED system used in this work is focused on careful evaluation of the chemical and environmental impacts of OAE,[39,40] and the release of alkalinity is restricted to large seawater tanks onshore, and CO_2 removal is not tracked. Considering that the BPMED system is unoptimized, we refrain from estimating overall process energy efficiency or CO_2 removal but rather focus on using it to source the waste acid. Only a portion (<25%) of the alkalinity is assumed to be used in the precipitation of Fe as shown in Fig. 1. As the BPMED system uses natural seawater and has all the necessary pre-treatment in place for eventual commercial deployment, the various types of waste and byproducts generated by the process are representative of future systems and relevant to our cost-benefit assessments.

A potential process to extract Ni from olivine (assumed 60 wt% in ultramafic rock ore) is shown in Fig. 1. The Ni concentration was estimated to be 2726 ppm based on experimental data. The productivity of Ni will be estimated based on the leaching time (2 weeks) and the overall recovery rate (39% for the base case, combining the leaching rate, precipitation rate, and plating rate) of Ni from experiments. The CO_2 capture in the stream containing Mg ions will be estimated based on the literature data.[41] The acid stream for the dissolution of olivine is

assumed to be provided by the BPMED system without any other cost except for fluid transport through pumps. Estimates of acid stream use came from published research on BPMED to generate the alkaline stream and acid stream.[42] The voltage of the Ni plating cell is assumed to be 3.5 V and the Ni recovery rate is taken from the literature results under this voltage.[43] The electricity consumption for Ni plating was estimated based on the Nernst equation and current efficiency from the literature.[43]

3. Results and discussion

Powder XRD patterns (Fig. 2a) of the as received olivine sample (Fig. 2c) matched with those of a previously reported olivine containing a Mg to Fe molar ratio of 92 to 8.[44] XRD measurements showed no other secondary crystalline phases, although the broad peaks in the low 2θ range suggest poor crystallinity in the sample that may arise due to impurities. To characterize the overall sample composition and its Ni content, the as received olivine was digested in acid and characterized by ICP-MS (Table 1).

Our analysis shows a Mg to Fe molar ratio of 92.4 to 7.6, which is consistent with our XRD analysis. Based on the major cation composition, the approximate molecular formula of the starting olivine is $Mg_{1.84}Fe_{0.16}SiO_4$. In addition to Mg and Fe, ICP analysis confirmed the presence of Ni, Mn, and Ca. The Ni present in the sample at 0.27 wt% is a typical concentration for highly forsteritic olivine which is reported to be between 0.2–0.4 wt%.[45] Given its fairly typical composition, our starting olivine sample serves as a good representative sample for investigating Ni extraction potential from olivine, although higher Ni containing olivine deposits are likely to be preferable from a process efficiency standpoint.

Particle size distribution of the as received olivine measured using a laser-based system (Fig. 2b) provided a D_{90} value of 147.1 μm with a median size of 82.91 μm. This median size is consistent with the average particle size of 79.6 μm obtained from analysis of optical microscopy images (Fig. 2d). The particle size distribution ranged from 1.76 μm to 312.12 μm (see Table S1). The particle size variability is expected to impact olivine dissolution rates, with smaller particles undergoing faster dissolution leaving larger particles behind that will dissolve at a slower rate. In fact, reducing average particle size is a common approach to increasing dissolution rates but it comes with the added energy cost of milling.[46] In this proof-of-concept study we do not reduce the particle size to optimize dissolution rates.

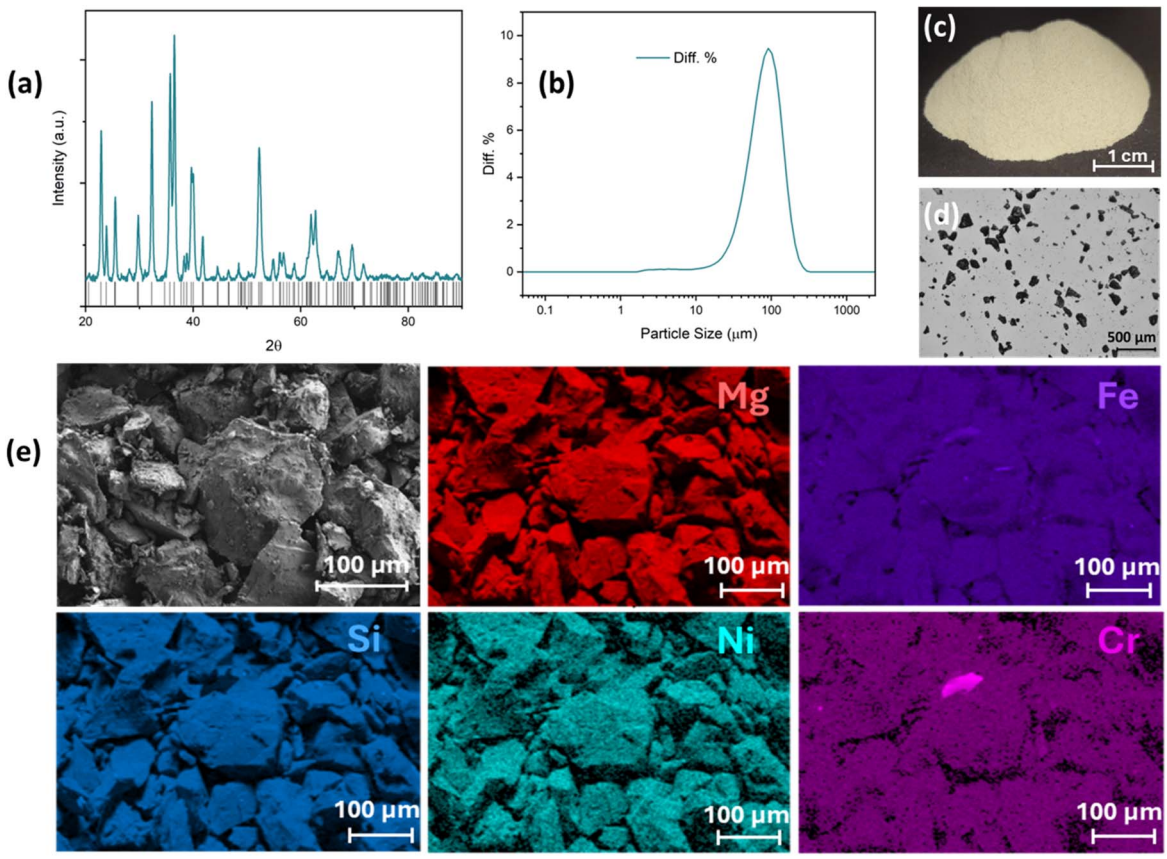

Fig. 2 Characterization of the olivine powder samples. (a) XRD of olivine samples with peak positions shown in gray for the previously reported olivine sample of composition $Mg_{1.84}Fe_{0.16}SiO_4$ (PDF# 98-000-3622). (b) Particle size measurement of the olivine powder sample. (c) Photograph of the as received olivine powder. (d) Optical image of olivine sample at 10× magnification. (e) SEM image and corresponding EDS maps showing the distribution of Mg, Fe, Si, Ni, and Cr in the sample.

Table 1 Weight percentage of elements in the olivine sample as determined by ICP-MS analysis

Element	Mg	Fe	Si	Mn	Ca	Ni
wt%	30.8%	5.80%	19.3%	0.08%	0.08%	0.27%

SEM and EDS characterization of the as received olivine (Fig. 2e) shows that Mg, Si, and Ni are well distributed throughout the sample with some small regions of higher Fe concentration. EDS mapping suggests that the Fe-rich regions correlate with higher concentrations of Cr and lower concentrations of Mg and Si, which suggests that the olivine may contain small quantities of a secondary crystalline chromite phase ($FeCr_2O_4$). Chromium was not detected by ICP-MS (detection limit of ~0.01 wt%), which is due to a combination of very low chromite content and inherent inhomogeneity of the sample. While we did not detect Cr by ICP-MS in the specific olivine samples used in this study, Cr release from olivine is an environmental concern,[31] and thus it is important to quantify and monitor Cr during olivine dissolution, especially when operating at a larger-scale. Another trace element previously targeted for extraction from olivine is cobalt (Co).[16] Given that we did not detect any Co by ICP-MS or EDS analysis in our specific olivine samples, we could not explore its separation, but note that it may be an element of interest in other olivine ores.

To assess the viability of utilizing BPMED generated acid, olivine dissolution experiments were conducted in parallel using both the BPMED acid and commercially sourced equimolar HCl. In terms of crystallinity and morphology characterized by XRD, the digestion of olivine in BPMED and HCl had similar effects (Fig. 3a). In both cases, the peaks in the sample become sharper and more defined compared to the starting sample after 24 hours, indicating a reduction in lattice strain that may be caused by the removal of small crystallite sizes from the sample and preferential leaching of defects during the dissolution experiment. Furthermore, differences in relative peak intensities were observed, suggesting that certain orientations of the particles undergo dissolution faster than others in the different acids, resulting in preferred orientation in the sample. Phase identification returned no new secondary crystalline phases after 24 hours of dissolution and the predominant phase was identified as forsterite. ICP-MS analysis was used to track the rate of dissolution for the major metal cations as shown in Fig. 3b–d. The rate of Mg and Fe dissolution over 24 hours is nearly identical with slightly faster leaching of Fe in both BPMED and HCl acid. Interestingly, the rate of dissolution of Ni is faster than that of Mg and Fe. This result is counter to what is reported in the literature.[18,47] As the Ni–O bond in olivine is shorter, and thus stronger than Mg–O and Fe–O bonds, Ni dissolution is expected to be slower. Given that the trend reversal is observed for both BPMED acid and commercial HCl, this result is likely due to the specific olivine sample studied, as different olivine sources will have different impurities and co-occurring phases and the specific Ni impurity type and location can alter lattice energy which impacts the relative leaching rates.[48] Beyond the individual element leaching rates, the

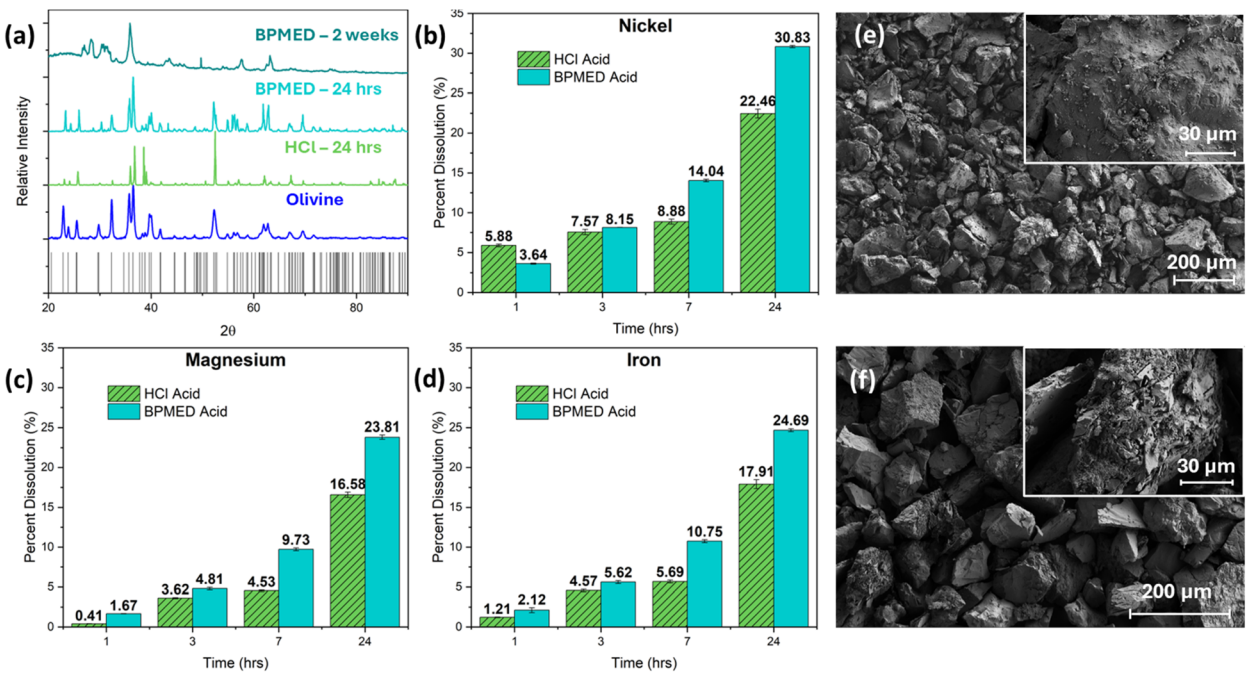

Fig. 3 Characterization of olivine leachate as a function of time and acid type. (a) XRD patterns of the as received olivine sample and solid residue left after acid digestion treatments. The ribbon plot comes from the expected pattern for $Mg_{1.84}Fe_{0.16}SiO_4$ (PDF# 98-000-3622). (b) Percent dissolution of Ni from the olivine sample in acid over time. (c) Percent dissolution of Mg from the olivine sample in acid over time. (d) Percent dissolution of Fe from the olivine sample in acid over time. (e) SEM images of olivine sample as received. (f) SEM images of olivine after exposure to BPMED acid for 24 hours. Inset in panels (e) and (f) show higher magnification images.

Table 2 ICP-MS quantification of cation concentration in leachate after 2 weeks of olivine digestion in BPMED acid

Element	Mg	Si	Fe	Ni
Percent dissolution (%)	88.5 ± 1.1	76.2 ± 1.8	88.9 ± 2.2	101.8 ± 2.6

comparison between the rates of BPMED and HCl acid shows that the BPMED acid leaches olivine at a faster rate than commercial HCl. Over 24 hours, BPMED acid leaches 37.3% more Ni, 43.6% more Mg, and 37.9% more Fe than commercial HCl. The increased rate of dissolution observed with BPMED acid is likely due to the higher ionic strength of the solution resulting from the trace amounts of residual salts (Table S2). Solutions with high ionic strength are known to enhance the activity coefficient of protons, and thus their reactivity, while the additional chloride ions have previously been shown to catalyze the acid leaching process.[49–51] To verify this underlying phenomenon, a dissolution experiment was conducted with a 4 g L^{-1} olivine loading in equal-strength HCl (pH 0.4) and increasing amounts of added NaCl (0, 0.1, and 1 M). After 24 hours, the mass of the residual olivine was measured to track the overall dissolution rates in the different NaCl-added leachate solutions. The dissolution of olivine was observed to increase with increasing ionic strength (*i.e.*, NaCl concentration). The percent dissolution of olivine was measured to be 18.6%, 22.4%, and 23.6% for leachate with 0, 0.1, and 1 M NaCl solutions, respectively (Table S3). Based on these results, and enhanced olivine leaching with BPMED acid *vs.* commercial HCl, subsequent experiments were solely conducted with BPMED acid.

To further characterize olivine dissolution, SEM and EDS imaging was conducted after 24 hours of exposure to BPMED acid (Fig. 3e and f). By comparing the SEM images, it is clear that acid digestion etches the olivine surface as evidenced by the pits and cracks present on the surface of the sample. In addition, the smaller olivine particles observed in the as received sample are completely absent from the digested sample which further supports the observed difference in the XRD patterns of the as received and acid treated olivine samples as the removal of small crystallites by digestion sharpens the peaks observed in XRD. The EDS mapping of the samples did not reveal a significant change in composition after 24 hours. Regions rich in Fe and Cr still remain that coincide with depleted regions of Mg and Si in the 24-hour sample. These regions are the remnants of the chromite phase detected in the starting olivine (Fig. S1). Ni itself appears to be well distributed throughout the sample with no significant changes observed.

To test the feasibility of extracting Ni from olivine using BPMED acid, a solution of 15 grams of olivine in 1 L of BPMED generated acid was left to digest at room temperature for 2 weeks to generate the feedstock. After 2 weeks, the residual solid collected weighed 1.38 grams, suggesting over 90% dissolution of the starting olivine (Fig. S2). The XRD pattern of the residual solid (Fig. 3a) indicates a structural change from the starting olivine, with peak broadening suggesting reduced crystallite sizes, and a bump in the pattern between 20° and 30° indicating the presence of significant amounts of amorphous phase, likely SiO_2. Close analysis of the XRD pattern identified the crystalline phase as a mixture of magnesioferrite ($MgFe_2O_4$) and enstatite ($MgSiO_3$) (Fig. S3).

The olivine leachate was characterized by ICP-MS to quantify the different cations released after the 2-week digestion period (Table 2). Our data show that 2 weeks is sufficient time to release nearly all of the Ni contained in the olivine into solution, even though not all of the olivine is fully digested. To selectively recover the Ni from solution, the Fe must be removed first as Ni and Fe have similar reduction potentials, making it difficult to reliably electroplate just Ni out of solution. To remove Fe, the pH of the solution was adjusted from a starting pH of ~1 to a pH of 6. The precipitates formed by increasing pH to 2, 3, 4, 5, and 6 are shown in Fig. 4a. Adjusting the pH from 1 to 3 induced little

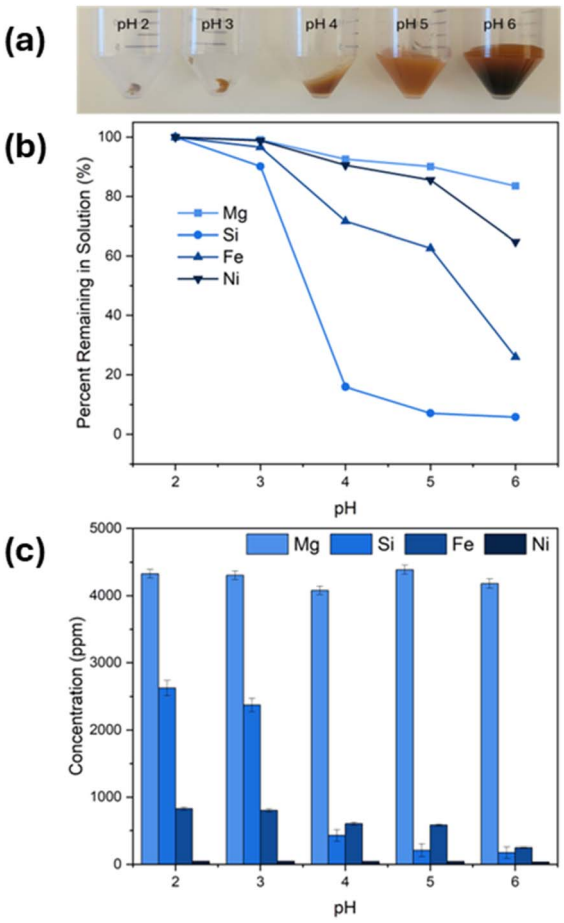

Fig. 4 (a) Precipitates generated by raising pH to the indicated threshold. (b) Percent of each species retained in the remaining solution after pH adjustment to the threshold. (c) Measured concentration of indicated species in the remaining solution.

precipitation with over 80% of each element still present in the solution after the pH adjustment (Fig. 4b). From pH 3 to pH 4, an appreciable amount of precipitate formed, removing the majority of the dissolved Si from solution and about ~30% of the Fe. This precipitation, however, also removed some of the leachate (2 vol%) entrapped in the gel that formed (Table S4). Gel formation continued from pH 4 to pH 5 accounting for an estimated total loss of 10 vol% of the starting leachate solution. Given that pH adjustment from 4 to 5 did not significantly alter the concentration of Mg and Ni (Fig. 4c), loss of solution volume to gel formation accounts for most of the observed Ni loss. Efforts to minimize gel formation *via* sequential precipitation, where precipitates are recovered at each pH setpoint, were tested but did not yield improved results (Fig. S4). Prior reports on minimizing gel formation in mineral extraction from silicate rocks have focused on minimizing the amount of dissolved silicon in solution.[52–54] Future optimization of this process will need to explore ways to minimize this gel formation, both to minimize loss of Ni and to facilitate easier handling of feedstock.

Upon further increasing the pH from 5 to 6, solid green precipitates rich in Fe were obtained. However, not all Fe is removed from solution at pH 6 as ICP-MS measurements show that ~25% of the starting Fe remains in solution (Fig. 4b). Note that increasing pH from 5 to 6 also leads to loss of Ni, likely due to co-precipitation with Fe oxyhydroxides. In total, the pH adjustments to remove Fe and Si from the leachate results in a loss of ~35% of the starting Ni, impacting overall Ni recovery. To mitigate the loss of Ni during the removal of Fe, a recent study explored the use of solvent extraction.[18] However, solvent extraction has undesirable environmental impacts, so we explored an alternative approach that does not need additional chemical inputs. Note that the green Fe precipitates contained Fe(II), which is highly water soluble, but Fe(II) can be easily oxidized to Fe(III) which is less water soluble. The Fe(II) to Fe(III) conversion can occur naturally over time or can be accelerated by increasing temperature or by adding an oxidizing agent like peroxide.[55] We used nominal heating of the leachate to accelerate Fe(II) oxidation. By heating the solution at 80 °C for 6 h we were able to remove additional Fe, as indicated by visible precipitates. Note that when the order of pH adjustment and oxidation was reversed, visual inspection showed significantly lower Fe precipitation. This difference is attributed to the higher effectiveness of Fe(II) in co-precipitating with Si than Fe(III). Once precipitated, subsequent removal of Si is achieved through absorption onto iron oxyhydroxides.[56] Through adjustment of pH to 6 followed by heat treatment, Fe in the leachate was mostly removed, and the remaining solution retained ~84% of the originally dissolved Mg and ~65% of the originally dissolved Ni for further processing.

Even with the removal of most major cations in the final leachate, the Ni concentration was ~34 ppm. At this concentration, the chemical precipitation of Ni is challenging due to low nucleation rates and slow kinetics of precipitation, contributing to overall unfavorable economics. Electrodeposition is a well-established technique that can selectively deposit the dissolved Ni as pure Ni-metal, which can be used in a diversity of applications. The large electrochemical window between Ni^{2+} ($Ni^{2+} + 2e^- \rightarrow Ni$, $E^\circ = -0.25$ V), Fe^{2+} ($Fe^{2+} + 2e^- \rightarrow Fe$, $E^\circ = -0.44$ V), and Mg^{2+} ($Mg^{2+} + 2e^- \rightarrow Mg$, $E^\circ = -2.37$ V) allows selective removal of Ni and Fe from solutions containing Mg, either as metals or FeNi alloy. As a proof of concept, Fig. 5a shows the cyclic voltammetry of the leachate solution. The cathodic peaks at −0.5 V and anodic peak at −0.35 V *vs.* Ag/AgCl are attributed to the reduction of Ni^{2+} and oxidation of Ni, respectively. The high current flow below −0.8 V is due to hydrogen evolution and reduction of Fe^{2+}. The strong anodic peaks at −0.6 V are attributed to the oxidation of Fe during the cathodic scan. Applying a constant voltage of −1.0 V *vs.* Ag/AgCl for 1 h (Fig. S5) deposits a thin layer of FeNi alloy on the surface of a Pt foil electrode (Fig. 5a inset). The XPS analysis (Fig. 5b and c) of the electrode confirmed the successful deposition of Ni and Fe containing species, likely Ni and Fe oxides. Surface oxidation of metals, especially Fe and Ni is expected and likely pronounced when the electrodeposits are thin. The composition of the electrodeposit based on XPS data showed a Ni to Fe ratio of 1 : 1.37. The Ni to Fe ratio in the alloy product can be altered through process control (electrolyte composition, pH, use of electrolyte additives, current densities, *etc.*).[57] For obtaining pure Ni-metal, the Fe in the electrolyte must be entirely removed, which can be accomplished using established solvent extraction methods, but would add to process costs.[18] In comparison, FeNi alloys, like the one recovered here, are suitable for the production of stainless steel, which accounts for the vast majority of Ni usage,[58] and are a valuable end-product (~$23 per kg^{-1}) from olivine that would not require such extensive chemical pretreatment for Fe removal.

The electrolyte after Ni recovery is a Mg-rich solution and can be used as an alkalinity source for OAE with nominal treatment. From previous literature, $Mg(OH)_2$ can be used to capture approximately 1.66 moles of CO_2 per mole of Mg.[34,59] For the process discussed here, the amount of CO_2 removed if 100% of the Mg is converted to $Mg(OH)_2$ is ~0.27 moles of CO_2 per liter. Dissolving more olivine or olivine with higher Mg content can

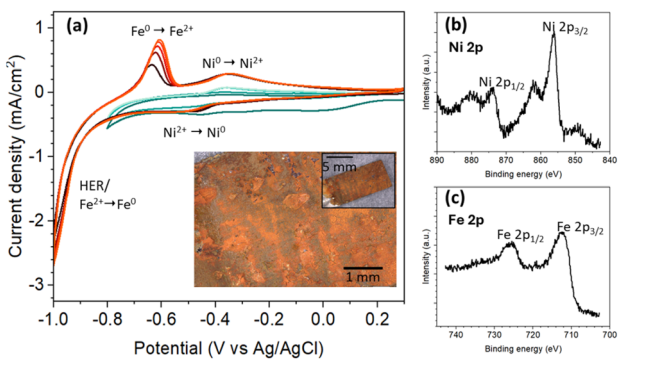

Fig. 5 Electrochemical extraction of Ni and Fe from the solution. (a) Cyclic voltammogram of the Pt electrode in olivine leachate solution (pH = 5) with different cut-off voltages. Inset optical images at varying magnifications of Pt electrode after 1 h deposition at −1.0 V *vs.* Ag/AgCl. (b) Ni 2p and (c) Fe 2p XPS spectra of the depositied film on the Pt electrode.

Table 3 Cost-benefit inputs and results for Ni recovery from olivine

Inputs	Value
Ultramafic ore (t h^{-1})	35
Olivine in ore	60%
Ni concentration in olivine (ppm)	2726
Ni leaching rate	97%
Ni precipitation rate	65%
Ni plating recovery rate	61.7%
Ni plating current efficiency	15.5%
Ni production (kg per t ore)	0.98
Electricity consumption (kWh per kg Ni)	5.36
Ni-metal price ($ per kg Ni)	31.72
Results	**Value**
Ni production cost ($ per kg)	15.07
CO_2 capture (kg per kg Ni)	335
Net benefit ($ per t ore)	16.32

further enhance the CO_2 capture potential of the residual Mg-rich stream.[60] Using the Mg-rich stream for OAE also minimizes waste streams generated by the Ni-recovery process.

Having successfully demonstrated the recovery of Ni as FeNi alloy from olivine, we estimated that the potential Ni produced from the pathway to be sufficient to support the growing demand for Ni-metal and Ni-containing alloys in the United States for more than 90 years (see the SI). For the BPMED-based Ni extraction presented here, the main benefit is from the Ni-metal or Ni-containing alloy recovery from a non-traditional Ni source with minimum waste streams generated and without the need for commodity acid and base solutions. The main cost is associated with electrical energy for the electroplating of Ni, pumping of processing fluids, and the equipment involved in the process. The net economic benefit and CO_2 capture capacity can be normalized to the mass of a metric ton of olivine ore, and the production cost of the Ni-metal is estimated by adding the electricity cost (normalized to mass of Ni) to annualized equipment costs (Table S5). The input parameters used in the cost-benefit analysis are summarized in Table 3. The Ni plating recovery rate and current efficiency were taken from the literature.[43] Using these parameters, the production cost of Ni was estimated to be $15.07 per kg Ni which is close to the current market price of Ni-metal ($16.41 per kg Ni) and lower than its price in 2022 ($31.72 per kg Ni). The CO_2 capture associated with producing 1 kg Ni using the proposed method, where the Mg-rich stream can be used for OAE, was calculated to be 335 kg—highlighting the environmental co-benefits of this extraction approach. The net economic benefit was estimated to be about +$16.32 per t ore without accounting for any carbon credits. While this absolute value seems low, our process which uses waste acid as a key input results in a +$24 per t ore higher economic benefit compared to a previously reported (−$8.1 per t ore) process that used commodity chemicals and accounted for carbon credits.[17] For the first time, our results show a pathway for net positive economic benefit for Ni recovery from olivine.

Given that this is a proof-of-concept study, and the process ended with a FeNi alloy, we compared the potential benefits of a couple of alternative scenarios to highlight the potential for additional economic benefits in the future. Taking the case with parameters shown in Table 3 as the base case, some variations in the key parameters, including the price and type of the product, the CO_2 credit, and the recovery rate led to different net benefits as shown in the summarized results (Table 4). Additionally, the higher overall recovery rate for Ni was estimated based on the assumption that all the Ni in the leachate would be collected during Ni plating. In the alloy product case, it was assumed that the product from the electrochemical plating is FeNi alloy, and the price was obtained online from an international vendor. The net benefit increases when the recovery rate of Ni and the potential CO_2 removal credit increase. In the meantime, it is also worth pointing out that the net economic benefit can drop significantly when the prices of the Ni products decrease. For the current process, the alloy product case is closest to what has been shown here. Given that the current price of Ni is low ($16.4 per kg^{-1} in 2025), process optimization to obtain pure Ni-metal would add additional costs without providing a significant economic benefit. Furthermore, generating high-purity Ni-metal will require minimizing the incorporation of trace metals such as Cr, Mn, and Co which could increase processing complexity and cost. In comparison, the FeNi alloy product for stainless steel production tolerates higher levels of trace metal impurities while being a comparable or higher value product ($23 per kg^{-1}).

The net benefit values compiled in Table 4 indicate that under the different scenarios, a net benefit of $1.31 per t ore to $32.76 per t ore can be achieved from the production of Ni or

Table 4 Comparison of the net benefit of Ni recovery from olivine in different cases[a]

Case	Ni price ($ per kg)	CO_2 credit ($ per t CO_2)	Overall recovery rate	Ni–Fe alloy ($ per kg)	Net benefit ($ per t ore)
Base	31.7	0	0.39	N/A	+16.32
High Ni recovery	31.7	0	0.60	N/A	+21.34
Low Ni price	16.4	0	0.39	N/A	+1.31
CO_2 credit[15]	31.7	50	0.39	N/A	+32.76
Alloy product	N/A	0	0.39	22.6	+7.39

[a] The low Ni price was taken from Trading Economics (March 2025).

FeNi alloy in a scaled-up process using equipment that processes 35 t ore per h. An advantage to the BPMED process is in the reduction of cost associated with the treatment and disposal of waste acid. Using the ore processing rate, the cost savings from averted acid treatment can be estimated. To process 35 tonnes of olivine per hour, about 1400 m^3 of the BPMED acid would be utilized. Previous estimates for waste disposal of dilute acid from a chemical industrial park place the cost of treating dilute acid at \$3.79 per m^3.[61] Utilizing the acid produced from BPMED for Ni recovery (40 m^3 per t ore) averts \$151.6 per t ore in acid waste treatment costs. Furthermore, the Mg-rich solution that remains after Ni recovery would require minimal treatment and neutralization to be a production stream for $Mg(OH)_2$ and $MgCO_3$, eliminating large volumes of liquid waste. Overall, the economics of scaling the BPMED system can be significantly enhanced by utilizing the waste acid for ore leaching and mineral recovery.

4. Conclusions

In this study we showed that BPMED-generated acid provides superior leaching performance compared to equal strength commercial HCl for digesting olivine. The acid digestion recovered over 90% of the Ni in the olivine, and with subsequent pH adjustment and nominal heating removed over 90% of the initial Fe and Si in solution. The remaining solution rich in Ni and Mg was used to electroplate and recover Ni as a FeNi alloy at a 39% overall process efficiency. Cost-benefit analysis showed that the net economic benefit of recovering Ni from olivine using the waste acid stream is +\$24 per t ore more compared to the literature. The net benefit depends on the price and type of the product, the CO_2 credit, and the recovery rate, all of which can be improved to produce a higher net economic benefit. This result indicates that our proof-of-concept Ni extraction pathway could be cost-effective and has the potential to become a carbon-negative process.

For future work, the process developed here will need to be optimized and generalized for a wide range of initial olivine compositions. Increasing the dissolution rate of the olivine can be a bottleneck and finding the optimal acid strength and solids loading will be critical to enhancing Ni recovery. If dissolution rates are an issue, acidic streams in the BPMED system can be recirculated for longer durations to increase their concentration to increase the digestion rate of olivine. Another general challenge would be the effective removal of silica to prevent gel formation. Investigating novel mixing conditions and optimizing process parameters could minimize silica gel issues. Further investigating various FeNi alloy compositions and optimizing electroplating to target higher value Ni alloys may improve process economics. While significant opportunities for optimization remain, Ni-metal recovery as a FeNi alloy from commercial olivine using waste acid from a demonstration-scale BPMED system deployed for ocean CO_2 sequestration highlights the feasibility and promise of integrating emerging technologies to effectively address our sustainable development and climate goals.

Author contributions

A. J. R. conducted olivine dissolution and precipitation experiments. D. T. N. conducted electrochemical Ni recovery experiments. J. L. conducted cost and emission calculations. B. A. and P. M. conducted ICP-MS and ICP-OES work, respectively. Q. W., P. B., and E. N. conducted SEM and EDS characterization. C. S. conceived the idea and designed the research, acquired funding, and supervised the project. All authors contributed to the discussion of experimental results and the review and editing of the manuscript.

Conflicts of interest

There are no conflicts to declare.

Data availability

The data supporting this article have been included as part of the supplementary information (SI). Supplementary information: further discussion on the methodology and sample preparation for ICP-MS and additional details on the technoeconomic analysis. Tables included in the SI show the size range of olivine (Table S1), the composition of major cations in BPMED acid (Table S2), dissolution of olivine in mineral acid solutions of varying ionic strength (Table S3), solution volume lost to gel formation at different pH thresholds (Table S4), and cost estimates for major equipment needed for the proposed process (Table S5). Figures in the SI show EDS analysis of olivine samples after 24 hours of dissolution (Fig. S1), photographs of the solution and solid residue from the bulk digestion experiment (Fig. S2), XRD of the solid residue after 2 weeks of digestion in BPMED acid (Fig. S3), photographs of the precipitates formed from pH adjustment (Fig. S4), the current profile of the electrodeposition (Fig. S5), XRD of the dried precipitates formed after pH adjustment (Fig. S6), photographs of the precipitate before and after heat treatment (Fig. S7), and XPS results from the electrodeposition experiment done before heat treatment (Fig. S8). See DOI: https://doi.org/10.1039/d5su00850f.

Acknowledgements

This work was supported in part by the U.S. Department of Energy, Water Power Technologies Office, at the Pacific Northwest National Laboratory (PNNL) through the Laboratory Research Program. We acknowledge partial support for this work from the Laboratory Directed Research and Development Program (LDRD) at PNNL under the under the Non-Equilibrium Transport Driven Separations Initiative (NETS). PNNL is a multiprogram national laboratory operated for DOE by Battelle under contract DE-AC05-76RLO1830. The authors acknowledge support for AJR under the ORISE Fellowship funded by the Water Power Technologies Office. Part of this work was conducted at the Molecular Analysis Facility, a National Nanotechnology Coordinated Infrastructure (NNCI) site at the University of Washington with partial support from the

National Science Foundation *via* awards NNCI-2025489 and NNCI-1542101. The authors thank Tyson Mink, Jeremy S. Loretz and Todd A. Pelman from Ebb Carbon, Inc. for providing samples of the BPMED feed and product streams used in the study.

References

1 P. Dilshara, B. Abeysinghe, R. Premasiri, N. Dushyantha, N. Ratnayake, S. Senarath, A. Sandaruwan Ratnayake and N. Batapola, The role of nickel (Ni) as a critical metal in clean energy transition: applications, global distribution and occurrences, production-demand and phytomining, *J. Asian Earth Sci.*, 2024, **259**, 105912, DOI: 10.1016/j.jseaes.2023.105912.

2 D. J. Bauer, R. T. Nguyen and B. J. Smith, *Critical Materials Assessment*, US Department of Energy, 2024.

3 G. Ragonnaud, *Critical Raw Materials Act*, EPRS, European Parliament, 2023.

4 J. Sun, H. Zhou and Z. Huang, The future nickel metal supply for lithium-ion batteries, *Green Chem.*, 2024, **26**(12), 6926–6943, DOI: 10.1039/D4GC01980F.

5 A. H. Pandyaswargo, A. D. Wibowo, M. F. N. Maghfiroh, A. Rezqita and H. Onoda, The emerging electric vehicle and battery industry in Indonesia: actions around the nickel ore export ban and a SWOT analysis, *Batteries*, 2021, **7**(4), 80.

6 H. U. Sverdrup and A. H. Olafsdottir, Assessing the long-term global sustainability of the production and supply for stainless steel, *Biophys Econ Resour Qual.*, 2019, **4**(2), 8, DOI: 10.1007/s41247-019-0056-9.

7 D. B. Nahon, H. Paquet and J. Delvigne, Lateritic weathering of ultramafic rocks and the concentration of nickel in the western Ivory Coast, *Econ. Geol.*, 1982, **77**(5), 1159–1175, DOI: 10.2113/gsecongeo.77.5.1159.

8 S. K. Som and R. Joshi, Chemical weathering of serpentinite and ni enrichment in fe oxide at sukinda area, jajpur district, orissa, india, *Econ. Geol.*, 2002, **97**(1), 165–172, DOI: 10.2113/gsecongeo.97.1.165.

9 R. Thorne, S. Roberts and R. Herrington, The formation and evolution of the bitincke nickel laterite deposit, albania, *Miner. Deposita*, 2012, **47**(8), 933–947, DOI: 10.1007/s00126-012-0411-x.

10 S. J. Barnes, Z.-S. Yao, Y.-J. Mao, A. P. Jesus, S. Yang, V. Taranovic and W. D. Maier, Nickel in olivine as an exploration indicator for magmatic Ni-Cu sulfide deposits: a data review and re-evaluation, *Am. Mineral.*, 2023, **108**(1), 1–17, DOI: 10.2138/am-2022-8327.

11 C. Butt and M. Elias, Nickel laterites: a review, *SEG Newsl.*, 2003, **54**, 1–18.

12 Y. W. Chiang, R. M. Santos, A. Van Audenaerde, A. Monballiu, T. Van Gerven and B. Meesschaert, Chemoorganotrophic bioleaching of Olivine for nickel recovery, *Minerals*, 2014, **4**(2), 553–564.

13 R. M. Santos, A. Van Audenaerde, Y. W. Chiang, R. I. Iacobescu, P. Knops and T. Van Gerven, Nickel extraction from olivine: effect of carbonation pre-treatment, *Metals*, 2015, **5**(3), 1620–1644.

14 F. Wang and D. Dreisinger, Carbon mineralization with concurrent critical metal recovery from olivine, *Proc. Natl. Acad. Sci. U. S. A.*, 2022, **119**(32), e2203937119.

15 F. Wang, D. Dreisinger and Y. Xiao, Accelerated CO2 mineralization and utilization for selective battery metals recovery from olivine and laterites, *J. Clean. Prod.*, 2023, **393**, 136345.

16 F. Wang and D. Dreisinger, An integrated process of CO2 mineralization and selective nickel and cobalt recovery from olivine and laterites, *Chem. Eng. J.*, 2023, **451**, 139002.

17 F. Wang and D. Dreisinger, Enhanced CO2 mineralization and selective critical metal extraction from olivine and laterites, *Sep. Purif. Technol.*, 2023, **321**, 124268, DOI: 10.1016/j.seppur.2023.124268.

18 N. Zhang, R. Yang, H. D. Huang, J. Meng, W. Zhang, A.-H. A. Park and A. Moment, Integrated recovery of iron and nickel from Olivine ores using solvent extraction: synergistic production of amorphous silica and carbonates through pH adjustment and carbon mineralization, *ACS ES&T Eng.*, 2025, **5**(1), 103–114, DOI: 10.1021/acsestengg.4c00462.

19 P. Meshram, Abhilash and B. D. Pandey, Advanced review on extraction of nickel from primary and secondary sources, *Miner. Process. Extr. Metall. Rev.*, 2019, **40**(3), 157–193, DOI: 10.1080/08827508.2018.1514300.

20 T. Khangaonkar, B. R. Carter, L. Premathilake, S. K. Yun, W. Ni, M. M. Stoll, N. D. Ward, L. G. Hemery, C. Torres Sanchez, C. V. Subban, *et al.*, Mixing and dilution controls on marine CO2 removal using alkalinity enhancement, *Environ. Res. Lett.*, 2024, **19**(10), 104039, DOI: 10.1088/1748-9326/ad7521.

21 K. Khoiruddin, I. G. Wenten and U. W. R. Siagian, Advancements in bipolar membrane electrodialysis techniques for carbon capture, *Langmuir*, 2024, **40**(18), 9362–9384, DOI: 10.1021/acs.langmuir.3c03873.

22 E. Cotter, R. Cavagnaro, A. Copping and S. Geerlofs, Powering negative-emissions technologies with marine renewable energy, in *OCEANS 2021: San Diego–Porto*, IEEE, 2021, pp. 1–8.

23 M. D. Eisaman, S. Geilert, P. Renforth, L. Bastianini, J. Campbell, A. W. Dale, S. Foteinis, P. Grasse, O. Hawrot, C. R. Löscher *et al.*, Assessing the technical aspects of ocean-alkalinity-enhancement approaches, *Guide to best practices in ocean alkalinity enhancement research*, 2023, vol. 2-oae2023, p. 3, DOI: 10.5194/sp-2-oae2023-3-2023.

24 F. Ferella, A. Suichies, B. A. Abdelkader, N. K. Dabhi, J. Werber and C.-F. de Lannoy, Ocean alkalinity enhancement using bipolar membrane electrodialysis: technical analysis and cost breakdown of a full-scale plant, *Ind. Eng. Chem. Res.*, 2025, **16**(13), 7085–7099, DOI: 10.1021/acs.iecr.4c04364.

25 S. Jin, M. D. Tyka, C. Rodriguez Martinez, C. E. Davis, C. Van Arsdale and A. R. Papania-Davis, Negative emission enabled by combining ocean alkalinity enhancement and waste

concrete upcycling, *ACS Sustain. Chem. Eng.*, 2025, **13**(4), 1532–1543, DOI: 10.1021/acssuschemeng.4c07507.

26 E. C. La Plante, X. Chen, S. Bustillos, A. Bouissonnie, T. Traynor, D. Jassby, L. Corsini, D. A. Simonetti and G. N. Sant, Electrolytic seawater mineralization and the mass balances that demonstrate carbon dioxide removal, *ACS ES&T Eng.*, 2023, **3**(7), 955–968, DOI: 10.1021/acsestengg.3c00004.

27 R. Schuiling and P. De Boer, Coastal spreading of olivine to control atmospheric CO2 concentrations: a critical analysis of viability. Comment: nature and laboratory models are different, *Int. J. Greenh. Gas Control*, 2010, **4**(5), 855.

28 G. Flipkens, M. Fuhr, G. Fiers, F. J. R. Meysman, R. M. Town and R. Blust, Enhanced olivine dissolution in seawater through continuous grain collisions, *Geochim. Cosmochim. Acta*, 2023, **359**, 84–99, DOI: 10.1016/j.gca.2023.09.002.

29 F. Montserrat, P. Renforth, J. Hartmann, M. Leermakers, P. Knops and F. J. R. Meysman, Olivine dissolution in seawater: implications for CO2 sequestration through enhanced weathering in coastal environments, *Environ. Sci. Technol.*, 2017, **51**(7), 3960–3972, DOI: 10.1021/acs.est.6b05942.

30 M. Fuhr, S. Geilert, M. Schmidt, V. Liebetrau, C. Vogt, B. Ledwig and K. Wallmann, Kinetics of Olivine weathering in seawater: an experimental study, *Front. Clim.*, 2022, **4**, 831587, DOI: 10.3389/fclim.2022.831587.

31 G. Flipkens, R. Blust and R. M. Town, Deriving nickel (Ni(II)) and chromium (Cr(III)) based environmentally safe Olivine guidelines for coastal enhanced silicate weathering, *Environ. Sci. Technol.*, 2021, **55**(18), 12362–12371, DOI: 10.1021/acs.est.1c02974.

32 B. Yang, J. Leonard and C. Langdon, Seawater alkalinity enhancement with magnesium hydroxide and its implication for carbon dioxide removal, *Mar. Chem.*, 2023, **253**, 104251.

33 C. A. Moras, T. Cyronak, L. T. Bach, R. Joannes-Boyau and K. G. Schulz, Effects of grain size and seawater salinity on magnesium hydroxide dissolution and secondary calcium carbonate precipitation kinetics: implications for ocean alkalinity enhancement, *Biogeosciences*, 2024, **21**(14), 3463–3475.

34 M. C. Ringham, N. Hirtle, C. Shaw, X. Lu, J. Herndon, B. R. Carter and M. D. Eisaman, An assessment of ocean alkalinity enhancement using aqueous hydroxides: kinetics, efficiency, and precipitation thresholds, *Biogeosciences*, 2024, **21**(15), 3551–3570, DOI: 10.5194/bg-21-3551-2024.

35 Ebb Carbon. https://www.ebbcarbon.com/ (Accessed October 2023).

36 Office, D. o. E. W. P. T., First-of-its-kind marine carbon dioxide removal device deployed in Washington State. https://www.energy.gov/eere/water/articles/first-its-kind-marine-carbon-dioxide-removal-device-deployed-washington-state (accessed).

37 J. R. Davis, *Nickel, Cobalt, and Their Alloys*, ASM International, 2000.

38 A. Taqieddin, S. Sarrouf, M. F. Ehsan, K. Buesseler and A. N. Alshawabkeh, Electrochemical ocean iron fertilization and alkalinity enhancement approach toward CO_2 sequestration, *npj Ocean Sustain.*, 2024, **3**(1), 28, DOI: 10.1038/s44183-024-00064-8.

39 K. Jones, L. Hemery, N. Ward, P. Regier, M. Ringham and M. Eisaman, *Biological Response of Eelgrass Epifauna, Taylor's Sea Hare (Phyllaplysia Taylori) and Eelgrass Isopod (Idotea Resecata), to Elevated Ocean Alkalinity*, EGUphere, 2024, pp. 1–25.

40 T. Khangaonkar, B. R. Carter, L. Premathilake, S. K. Yun, W. Ni, M. M. Stoll, N. D. Ward, L. G. Hemery, C. T. Sanchez and C. V. Subban, Mixing and dilution controls on marine CO_2 removal using alkalinity enhancement, *Environ. Res. Lett.*, 2024, **19**(10), 104039.

41 J. Griffioen, Enhanced weathering of olivine in seawater: the efficiency as revealed by thermodynamic scenario analysis, *Sci. Total Environ.*, 2017, **575**, 536–544, DOI: 10.1016/j.scitotenv.2016.09.008.

42 F. Ferella, A. Suichies, B. A. Abdelkader, N. K. Dabhi, J. Werber and C.-F. de Lannoy, Ocean alkalinity enhancement using bipolar membrane electrodialysis: technical analysis and cost breakdown of a full-scale plant, *Ind. Eng. Chem. Res.*, 2025, **64**(13), 7085–7099, DOI: 10.1021/acs.iecr.4c04364.

43 P. M.-U. N. Laokhen, T. Yingnakorn, T. Patcharawit and S. Khumkoa, Recovery of nickel from spent electroplating solution by hydrometallurgical and electrometallurgical process, *J. Met., Mater. Miner.*, 2022, **32**, 95–100, DOI: 10.55713/jmmm.v32i2.1253.

44 M. Merli, R. Oberti, F. Caucia and L. Ungaretti, Determination of site population in olivine: warnings on X-ray data treatment and refinement, *Am. Mineral.*, 2001, **86**(1–2), 55–65.

45 T. Simkin and J. V. Smith, Minor-element distribution in Olivine, *J. Geol.*, 1970, **78**(3), 304–325.

46 S. Foteinis, J. S. Campbell and P. Renforth, Life cycle assessment of coastal enhanced weathering for carbon dioxide removal from air, *Environ. Sci. Technol.*, 2023, **57**(15), 6169–6178, DOI: 10.1021/acs.est.2c08633.

47 Y. Liu, A. A. Olsen and J. D. Rimstidt, Mechanism for the dissolution of olivine series minerals in acidic solutions, *Am. Mineral.*, 2006, **91**(2–3), 455–458.

48 M. Sassi and S. N. Kerisit, Ni and Co incorporation in forsterite: a density functional theory study with hubbard correction, *ACS Earth Space Chem.*, 2024, **8**(5), 1027–1038, DOI: 10.1021/acsearthspacechem.3c00370.

49 Z. Abbas and E. Ahlberg, Activity coefficients of concentrated salt solutions: a monte carlo investigation, *J. Solution Chem.*, 2019, **48**(8), 1222–1243, DOI: 10.1007/s10953-019-00905-y.

50 G. Senanayake, Review of theory and practice of measuring proton activity and pH in concentrated chloride solutions and application to oxide leaching, *Miner. Eng.*, 2007, **20**(7), 634–645, DOI: 10.1016/j.mineng.2007.01.002.

51 L. Wang, S. Yin, B. Deng and A. Wu, Copper sulfides leaching assisted by acidic seawater-based media: ionic strength and

mechanism, *Miner. Eng.*, 2022, **175**, 107286, DOI: 10.1016/j.mineng.2021.107286.

52 G. M. Tsaousi, A. Toli, A. Bempelou, D. Kotsanis, M. Vafeias, E. Balomenos and D. Panias, Control of silica gel formation in the acidic leaching of calcium aluminate slags with aqueous HCl for Al extraction, *Sustainability*, 2023, **15**(21), 15462.

53 I. Silin, C. Dertmann, V. S. Cvetković, S. Stopic and B. Friedrich, Prevention of silica gel formation for eudialyte study using new digestion reactor, *Minerals*, 2024, **14**(2), 124.

54 C. Matus, S. Stopic, S. Etzold, D. Kremer, H. Wotruba, C. Dertmann, R. Telle, B. Friedrich and P. Knops, Mechanism of nickel, magnesium, and iron recovery from olivine bearing ore during leaching with hydrochloric acid including a carbonation pre-treatment, *Metals*, 2020, **10**(6), 811.

55 J. Huang, A. Jones, T. D. Waite, Y. Chen, X. Huang, K. M. Rosso, A. Kappler, M. Mansor, P. G. Tratnyek and H. Zhang, Fe(II) redox chemistry in the environment, *Chem. Rev.*, 2021, **121**(13), 8161–8233, DOI: 10.1021/acs.chemrev.0c01286.

56 L. Huang, C. T. Parsons, S. Slowinski and P. Van Cappellen, Co-precipitation of iron and silicon: reaction kinetics, elemental ratios and the influence of phosphorus, *Chemosphere*, 2024, **349**, 140930, DOI: 10.1016/j.chemosphere.2023.140930.

57 V. Torabinejad, M. Aliofkhazraei, S. Assareh, M. H. Allahyarzadeh and A. S. Rouhaghdam, Electrodeposition of Ni-Fe alloys, composites, and nano coatings–a review, *J. Alloys Compd.*, 2017, **691**, 841–859, DOI: 10.1016/j.jallcom.2016.08.329.

58 Nickel and nickel alloys, in *Metals Handbook Desk Edition*, ASM International, 1998, DOI: 10.31399/asm.hb.mhde2.a0003147.

59 J. He and M. D. Tyka, Limits and CO2 equilibration of near-coast alkalinity enhancement, *Biogeosciences*, 2023, **20**(1), 27–43, DOI: 10.5194/bg-20-27-2023.

60 V. Kitidis, S. A. Rackley, W. J. Burt, G. H. Rau, S. Fawcett, M. Taylor, G. Tarran, E. M. S. Woodward, C. Harris and T. Fileman, Magnesium hydroxide addition reduces aqueous carbon dioxide in wastewater discharged to the ocean, *Commun. Earth Environ.*, 2024, **5**(1), 354, DOI: 10.1038/s43247-024-01506-4.

61 Y. Lyu, H. Ye, Z. Zhao, J. Tian and L. Chen, Exploring the cost of wastewater treatment in a chemical industrial Park: model development and application, *Resour. Conserv. Recycl.*, 2020, **155**, 104663, DOI: 10.1016/j.resconrec.2019.104663.